Chapter 8
Generation and Applications of Squeezed Light

Abstract In this chapter we shall describe how the squeezing spectrum may be calculated for intracavity nonlinear optical processes. We shall confine the examples to processes described by an effective Hamiltonian where the medium is treated classically. We are able to extend the treatment o squeezing in the parametric oscillator to the above threshold regime. In addition, we calculate the squeezing spectrum for second harmonic generation and dispersive optical bistability. We also consider the non degenerate parametric oscillator where it is possible to achieve intensity fluctuations below the shot-noise level for the difference in the signal and idle intensities. Two applications of squeezed light will be discussed: interferometric detection of gravitational radiation and sub-shot-noise phase measurements.

8.1 Parametric Oscillation and Second Harmonic Generation

We consider the interaction of a light mode at frequency ω_1 with its second harmonic at frequency $2\omega_1$. The nonlinear medium is placed within a Fabry–Perot cavity driven coherently either at frequency $2\omega_1$ (parametric oscillation or frequency ω_1 (second harmonic generation)). We shall begin by including driving fields both at frequency ω_1 and $2\omega_1$ so that both situations may be described within the one formalism. We write the Hamiltonian as [1]

$$\begin{aligned}
&\mathscr{H} = \mathscr{H}_1 + \mathscr{H}_2 \,, \\
&\mathscr{H}_1 = \hbar\omega_1 a_1^\dagger a_1 + 2\hbar\omega_1 a_2^\dagger a_2 + \mathrm{i}\frac{\hbar\kappa}{2}(a_1^{\dagger 2} a_2 - a_1^2 a_2^\dagger) + \mathrm{i}\hbar(E_1 a_1^\dagger \, \mathrm{e}^{-\mathrm{i}\omega_1 t}) \\
&\qquad - E_1^* a_1 \mathrm{e}^{\mathrm{i}\omega_1 \mathrm{t}}) + \mathrm{i}\hbar(E_2 a_2^\dagger \mathrm{e}^{-2\mathrm{i}\omega_1 t} - E_2^* a_2 \mathrm{e}^{2\mathrm{i}\omega_1 t}) \,, \\
&\mathscr{H}_2 = a_1 \Gamma_1^\dagger + a_1^\dagger \Gamma_1 + a_2 \Gamma_2^\dagger + a_2^\dagger \Gamma_2 \,,
\end{aligned}$$

where a_1 and a_2 are the Boson operators for modes of frequency ω_1 and $2\omega_1$, respectively, κ is the coupling constant for the interaction between the two modes and

the spatial mode functions are chosen so that κ is real, Γ_1, Γ_2 are heat bath operators which represent cavity losses for the two modes and E_1 and E_2 are proportional to the coherent driving field amplitudes.

The master equation for the density operator of the two cavity modes after tracing out over the reservoirs is

$$\frac{\partial \rho}{\partial t} = \frac{1}{\mathrm{i}\hbar}[\mathscr{H}_1,\ \rho] + (L_1 + L_2)\rho\ , \tag{8.2}$$

where

$$L_i\rho = \gamma_i(2a_i\rho a_i^\dagger - a_i^\dagger a_i\rho - \rho a_i^\dagger a_i)\ ,$$

and γ_i are the cavity damping rates of the modes.

This master equation may be converted to a c-number Fokker–Planck equation in the generalised P representation. The generalised P representation must be used since the c-number equation would have a non-positive definite diffusion matrix if the Glauber–Sudarshan P representation were used. The result is

$$\begin{aligned}\frac{\partial}{\partial t}P(\boldsymbol{a}) = \Bigg\{ & \frac{\partial}{\partial \alpha_1}(\gamma_1\alpha_1 - E_1 - \kappa\alpha_1^\dagger\alpha_2) + \frac{\partial}{\partial \alpha_1^\dagger}(\gamma_1\alpha_1^\dagger - E_1^* - \kappa\alpha_1\alpha_2^\dagger) \\ & + \frac{\partial}{\partial \alpha_2}\left(\gamma_2\alpha_2 - E_2 + \frac{\kappa}{2}\alpha_1^2\right) + \frac{\partial}{\partial \alpha_2^\dagger}\left(\gamma_2\alpha_2^\dagger - E_2^* + \frac{\kappa}{2}\alpha_1^{\dagger 2}\right) \\ & + \frac{1}{2}\left[\frac{\partial^2}{\partial \alpha_1^2}(\kappa\alpha_2) + \frac{\partial^2}{\partial \alpha_1^{\dagger 2}}(\kappa\alpha_2^\dagger)\right]\Bigg\} P(\boldsymbol{a})\ ,\end{aligned} \tag{8.3}$$

where $\boldsymbol{a} = [\alpha_1,\ \alpha_1^\dagger,\ \alpha_2,\ \alpha_2^\dagger]$, and we have made the following transformation to the rotating frames of the driving fields

$$\alpha_1 \to \alpha_1 \exp(-\mathrm{i}\omega_1 t), \qquad \alpha_2 \to \alpha_2 \exp(-2\mathrm{i}\omega_1 t)\ .$$

In the generalized P representation α and $\alpha^\dagger$ are independent complex variables and the Fokker–Planck equation has a positive semi-definite diffusion matrix in an eight-dimensional space. This allows us to define equivalent stochastic differential equations using the Ito rules

$$\frac{\partial}{\partial t}\begin{pmatrix}\alpha_1 \\ \alpha_1^\dagger\end{pmatrix} = \begin{pmatrix}E_1 + \kappa\alpha_1^\dagger\alpha_2 - \gamma_1\alpha_1 \\ E_1^* + \kappa\alpha_1\alpha_2^\dagger - \gamma_1\alpha_1^\dagger\end{pmatrix} + \begin{pmatrix}\kappa\alpha_2 & 0 \\ 0 & \kappa\alpha_2^\dagger\end{pmatrix}^{1/2}\begin{pmatrix}\eta_1(t) \\ \eta_1^\dagger(t)\end{pmatrix}\ , \tag{8.4}$$

$$\frac{\partial}{\partial t}\begin{pmatrix}\alpha_2 \\ \alpha_2^\dagger\end{pmatrix} = \begin{pmatrix}E_2 - \frac{\kappa}{2}\alpha_1^2 - \gamma_2\alpha_2 \\ E_2^* - \frac{\kappa}{2}\alpha_1^{\dagger 2} - \gamma_2\alpha_2^\dagger\end{pmatrix}\ , \tag{8.5}$$

where $\eta_1(t),\ \eta_1^\dagger(t)$ are delta correlated stochastic forces with zero mean, namely

$$\begin{aligned}\langle \eta_1(t)\rangle &= 0\\ \langle \eta_1(t)\eta_1(t')\rangle &= \delta(t-t')\\ \langle \eta_1(t)\eta^{\dagger}(t')\rangle &= 0\,.\end{aligned} \tag{8.6}$$

8.1.1 Semi-Classical Steady States and Stability Analysis

The semi-classical or mean value equations follow directly from (8.4 and 8.5) with the replacement of $\alpha_i^{\dagger}$ by α_i^*.

$$\frac{\partial}{\partial t}\alpha_1 = E_1 + \kappa\alpha_1^*\alpha_2 - \gamma_1\alpha_1\,, \tag{8.7}$$

$$\frac{\partial \alpha_2}{\partial t} = E_2 + \frac{\kappa}{2}\alpha_1^2 - \gamma_2\alpha_2\,. \tag{8.8}$$

We shall investigate the steady states of these equations and their stability. The stability of the steady states may be determined by a linearized analysis for small perturbations around the steady state

$$\alpha_1 = \alpha_1^0 + \delta\alpha_1\,, \qquad \alpha_2 = \alpha_2^0 + \delta\alpha_2\,, \tag{8.9}$$

where α_1^0, α_2^0 are the steady-state solutions of (8.7 and 8.8). The linearized equations for the fluctuations are

$$\frac{\partial}{\partial t}\begin{pmatrix}\delta\alpha_1\\ \delta\alpha_1^*\\ \delta\alpha_2\\ \delta\alpha_2^*\end{pmatrix} = \begin{pmatrix}-\gamma_1 & \kappa\alpha_2^0 & \kappa\alpha_1^0 & 0\\ \kappa\alpha_2^{0^*} & -\gamma_1 & 0 & \kappa\alpha_1^0\\ -\kappa\alpha_1^{0^*} & 0 & -\gamma_2 & 0\\ 0 & -\kappa\alpha_1^{0^*} & 0 & -\gamma_2\end{pmatrix}\begin{pmatrix}\delta\alpha_1\\ \delta\alpha_1^*\\ \delta\alpha_2\\ \delta\alpha_2^*\end{pmatrix}\,. \tag{8.10}$$

The four eigenvalues of these equations are

$$\begin{aligned}\lambda_1,\,\lambda_2 &= -\frac{1}{2}(-|\kappa\alpha_2^0| + \gamma_1 + \gamma_2) \pm \frac{1}{2}[(-|\kappa\alpha_2^0| + \gamma_1 - \gamma_2)^2 - 4|\kappa\alpha_1^0|^2]^{1/2}\,,\\ \lambda_3,\,\lambda_4 &= -\frac{1}{2}(|\kappa\alpha_2^0| + \gamma_1 + \gamma_2) \pm \frac{1}{2}[(|\kappa\alpha_2^0| + \gamma_1 - \gamma_2)^2 - 4|\kappa\alpha_1^0|^2]^{1/2}\,.\end{aligned} \tag{8.11}$$

The fixed points become unstable when one or more of these eigenvalues has a positive real part. If a fixed point changes its stability as one of the parameters is varied we call this a bifurcation. In this problem the nature of bifurcations exhibited come in many forms including a fixed point to limit cycle transition.

We shall consider the cases of parametric oscillation and second harmonic generation separately.

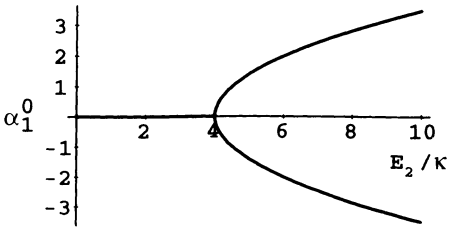

Fig. 8.1 Steady state amplitude of the fundamental mode versus pump field amplitude for parametric oscillation, $\kappa = 1.0$, $E_2^c = 4.0$

8.1.2 Parametric Oscillation

For parametric oscillation only the mode at frequency $2\omega_1$ is pumped so we set $E_1 = 0$. The stable steady state solutions for the mode amplitudes are below threshold $E_2 < E_2^c$

$$\alpha_1^0 = 0, \qquad \alpha_2^0 = \frac{E_2}{\gamma_2}\,, \tag{8.12}$$

above threshold $E_2 > E_2^c$

$$\alpha_1^0 = \pm\left[\frac{2}{\kappa}(E_2 - E_2^c)\right]^{1/2}, \qquad \alpha_2^0 = \frac{\gamma_1}{\kappa}\,, \tag{8.13}$$

where $E_2^c = \gamma_1\gamma_2/\kappa$, and we have taken E_2 to be positive. Thus the system exhibits behaviour analogous to a second-order phase transition at $E_2 = E_2^c$ where the below-threshold solution $\alpha_1^0 = 0$ becomes unstable and the system moves onto a new stable branch. Above threshold there exist two solutions with equal amplitude and opposite phase. In Fig. 8.1 we plot the amplitude α_1^0 versus E_2.

8.1.3 Second Harmonic Generation

For second harmonic generation only the cavity mode at frequency ω is pumped so we set $E_2 = 0$. Equations (8.7 and 8.8) then yield the following equation for the steady state amplitude of the second harmonic

$$-2\gamma_2(\kappa\alpha_2^0)^3 + 4\gamma_1\gamma_2(\kappa\alpha_2^0) - 2\gamma_1^2\gamma_2(\kappa\alpha_2^0) = |\kappa E_1|^2\,. \tag{8.14}$$

This gives a solution for α_2^0 which is negative and the intensity $|\alpha_2^0|^2$ is a monotonically increasing, single valued function of $|E_1|^2$.

However from the stability analysis we find that the eigenvalues

$$\lambda_1,\ \lambda_2 \to 0 \pm \mathrm{i}\omega\,, \tag{8.15}$$

where $\omega = [\gamma_2(2\gamma_1 + \gamma_2)]^{1/2}$ when the driving field E_1 reaches the critical value

$$E_1^c = \frac{1}{\kappa}(2\gamma_1 + \gamma_2)[2\gamma_2(\gamma_1 + \gamma_2)]^{1/2} . \tag{8.16}$$

Thus the light modes in the cavity undergo a hard mode transition, where the steady state given by (8.14) becomes unstable and is replaced by periodic limit cycle behaviour. This behaviour is illustrated in Fig. 8.2 which shows the time development of the mode intensities above the instability point.

8.1.4 Squeezing Spectrum

We shall calculate the squeezing spectrum using a linearized fluctuation analysis about the steady state solutions [2, 3]. The linearized drift and diffusion matrices for the Fokker–Planck equation (8.3) are

$$A = \begin{pmatrix} \gamma_1 & -\varepsilon_2 & -\varepsilon_1^* & 0 \\ -\varepsilon_2^* & \gamma_1 & 0 & -\varepsilon_1 \\ \varepsilon_1 & 0 & \gamma_2 & 0 \\ 0 & \varepsilon_1^* & 0 & \gamma_2 \end{pmatrix} , \tag{8.17}$$

$$D = \begin{pmatrix} \varepsilon_2 & 0 & 0 & 0 \\ 0 & \varepsilon_2^* & 0 & 0 \\ 0 & 0 & 0 & 0 \\ 0 & 0 & 0 & 0 \end{pmatrix} . \tag{8.18}$$

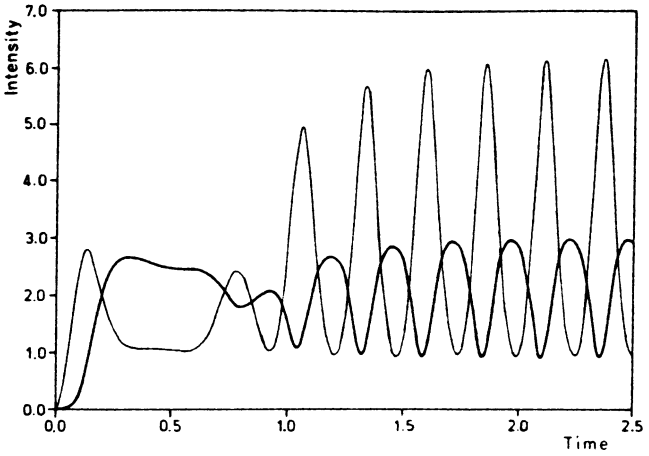

Fig. 8.2 Self pulsing in second harmonic generation: $|\alpha_1|^2$ (light), $|\alpha_2|^2$ (heavy) as functions of time. Numerical solutions of (8.7 and 8.8) with $\kappa = 10.0,\ \gamma_1 = \gamma_2 = 3.4,\ \varepsilon_1 = 20.0,\ \varepsilon_2 = 0.0$ and initial conditions $\alpha_1 = 0.1 + 0.1\mathrm{i},\ \alpha_2 = 0.0$

where $\varepsilon_2 = \kappa\alpha_2^0$, $\varepsilon_1 = \kappa\alpha_1^0$, and we have replaced α_2 in the diffusion matrix by its steady state value. We may then use (7.72) to calculate the spectral matrix $S(\omega)$.

The results for the squeezing in the amplitude and phase quadratures follow from (8.17 and 8.18). The squeezing in the low frequency mode (ω_1) is

$$S_{1\pm}^{\text{out}}(\omega) = 1 \pm \frac{4\gamma_1|\varepsilon_2|(\gamma_2^2+\omega^2)}{[\gamma_2(\gamma_1 \mp |\varepsilon_2|) + |\varepsilon_1|^2 - \omega^2]^2 + \omega^2(\gamma_1 \mp |\varepsilon_2| + \gamma_2)^2} , \tag{8.19}$$

where the $+$ and $-$ refer to the unsqueezed and squeezed quadratures, respectively. The squeezing in the high frequency mode $(2\omega_1)$ is

$$S_{2\pm}^{\text{out}}(\omega) = 1 \pm \frac{4\gamma_2|\varepsilon_2||\varepsilon_1|^2}{[\gamma_2(\gamma_1 \mp |\varepsilon_2|) + |\varepsilon_1|^2 - \omega^2]^2 + \omega^2(\gamma_1 \mp |\varepsilon_2| + \gamma_2)^2} , \tag{8.20}$$

The above results are general for two driving field ε_1 and ε_2. We now consider the special cases of parametric oscillation and second harmonic generation.

8.1.5 Parametric Oscillation

For parametric oscillation $\varepsilon_1 = 0$ and below threshold the expression for the squeezing spectrum simplifies considerably. The phase quadrature is squeezed with

$$S_{1-}^{\text{out}}(\omega) = 1 - \frac{4\gamma_1|\varepsilon_2|}{(\gamma_1 + |\varepsilon_2|)^2 + \omega^2} . \tag{8.21}$$

This is a Lorentzian dip below the vacuum level which as threshold is approached $|\varepsilon_2| = \gamma$ gives $S_1^{\text{out}} - (0) = 0$. This is the same result as obtained in Chap. 7 where the pump mode was treated classically. However, this treatment also allows us to investigate the above-threshold regime. The squeezing spectrum above threshold becomes double peaked for

$$|\varepsilon_1|^2 > \gamma_2^2\{[\gamma_2^2 + (\gamma_2 + 2\gamma_1)^2]^{1/2} - (\gamma_2 + 2\gamma_1)\} . \tag{8.22}$$

The double-peaked squeezing spectrum is plotted in Fig. 8.3. If the high-frequency losses from the cavity are insignificant $(\gamma_2 \ll \gamma_1)$, this splitting occurs immediately above threshold, with the greatest squeezing being at $\omega = \pm|\varepsilon_1|$. The value of $S_1^{\text{out}} - (|\varepsilon_1|)$ remains close to zero even far above threshold. In Fig. 8.4 we plot the maximum squeezing obtained as a function of $|\varepsilon_1|$ for different values of the ratio of the cavity losses γ_2/γ_1. Below threshold the squeezing is independent of this ratio but above threshold the squeezing depends crucially on this ratio. Above threshold the pump is depleted, and noise from the pump enters the signal field. If the cavity losses at the pump frequency are significant, then uncorrelated vacuum fluctuations will feed through into the signal and degrade the squeezing. Thus a low

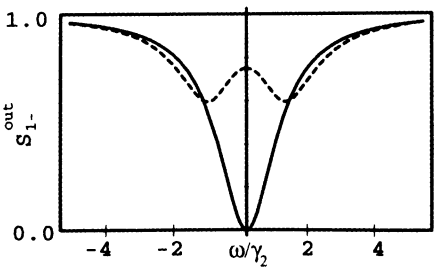

Fig. 8.3 The squeezing spectrum for parametric oscillation with $\gamma_1 = 2\gamma_2$. *Solid line*: on threshold with $\varepsilon_2 = \gamma_1$. *Dashed line*: above threshold with $\varepsilon_1 = \gamma_2$

cavity loss at the pump frequency by comparison with the signal loss is needed to obtain good squeezing above threshold in the parametric oscillator.

We may also consider the squeezing in the pump mode. Below threshold this mode is not squeezed. Above threshold the peak squeezing (at $\omega = 0$) increases to a maximum value of 50% at $|\varepsilon_1| = 2\gamma_1\gamma_2$. When $|\varepsilon_1| = 2\gamma_1^2 + \frac{1}{2}\gamma_2^2$, we again find a splitting into a double peak.

8.1.6 Experiments

The first experiment to demonstrate the generation of squeezed light in an optical parametric oscillator below threshold was been performed by *Wu* et al. [4]. They demonstrated reductions in photocurrent noise greater than 60% (4 dB) below the limit set by the vacuum fluctuations of the field are observed in a balanced homodyne detector. *Lam* et al. [5] reported 7 dB of measured vacuum squeezing. A schematic of their experiment is shown in Fig. 8.5. The experiment used a monolithic MgO:$LiNbO_3$ nonlinear crystal as the nonlinear medium. This was pumped at a wavelength of 532 nm from a second harmonic source (a hemilithic crystal of MgO:$LiNbO_3$). Squeezed light is generated at 1064nm. The squeezing cavity output coupler is 4% reflective to 532 nm and 95.6% reflective to 1064 nm. The other end is a high reflector with 99.96% for both wavelengths. The cavity finesse was $F = 136$, and a free spectral range $FSR = 9$ GHz. The cavity linewidth was 67 MHz. The output of the OPO is directed to a pure TEM_{00} mode cleaning cavity with a

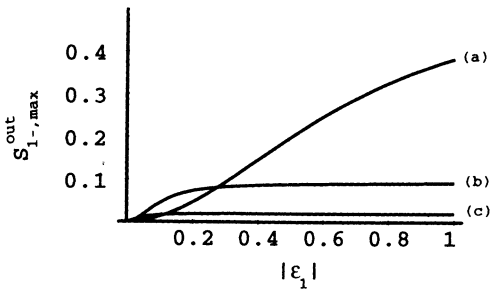

Fig. 8.4 Maximum squeezing above threshold as a function of the amplitude of the fundamental mode $|\varepsilon_1|$, for different values of the cavity losses γ_2/γ_1; (a) 0.02, (b) 0.1, (c) 1.0

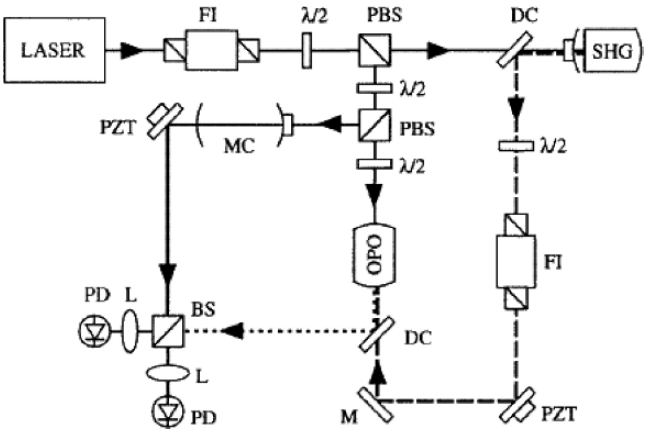

Fig. 8.5 The experimental scheme of Lam et al. for producing vacuum squeezing in an optical parametric oscillator below threshold. Solid, dashed and dotted lines are the 1,064 nm laser, second harmonic and vacuum squeezed light beams, respectively. M: mirror, FI: Faraday isolator, PZT: piezo-electric actuator, DC: dichroic beamsplitter, L: lens, PD: photodetector, (P)BS: (polarizing) beamsplitter, $'/2$: half-wave plate, SHG: second-harmonic generator and MC: mode cleaner cavity

finesse of 5,000 and a line width of 176 kHZ. This allows the squeezing generated by the OPO to be optimized by tuning the mode cleaner length. The final homodyne detection used a pair of ETX-500 InGaAs photodiodes with a quantum efficiency of 0.94 ± 0.02 and a 6 mW optical local oscillator. The dark noise of the photodetectors

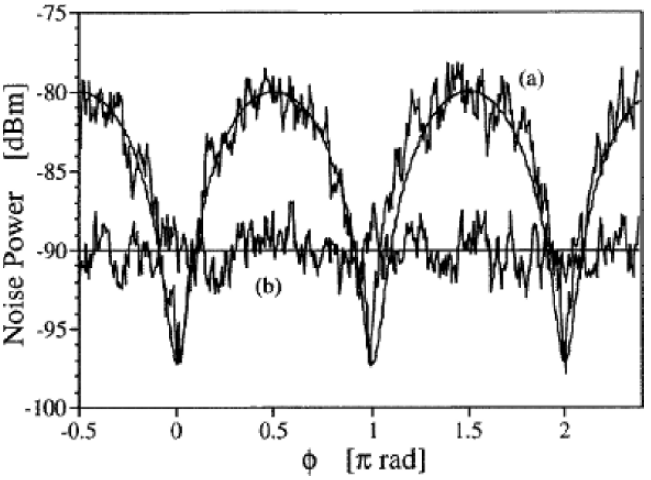

Fig. 8.6 Quadrature variance of the squeezed vacuum. Trace (a) shows experimental results of the variance of the squeezed vacuum state as a function of local oscillator phase. The smooth line is fitted values of a 7.1 dB squeezed vacuum assuming the given experimental efficiencies. In curve (b) is the standard quantum noise level at -90 dB

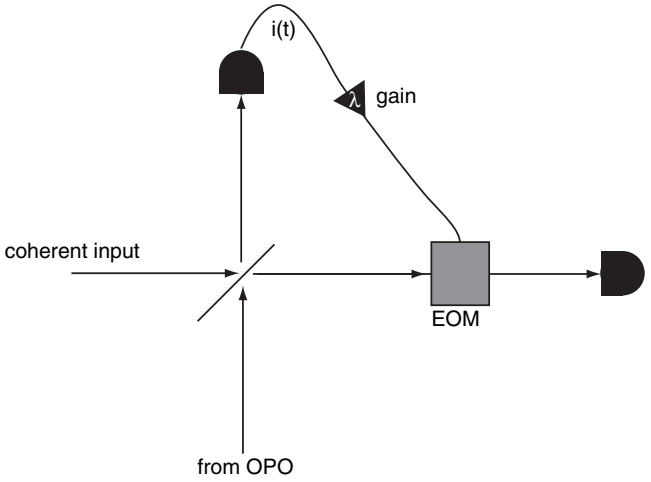

Fig. 8.7 An electro-optic feed-forward scheme used by Lam et al. to produce a bright squeezed state. The electro-optic modulator (EOM) is controlled be the photo-current $i(t)$

was 10 dB below the measured vacuum quantum noise level and hence the squeezed vacuum measurement does not require any electronic noise floor correction.

In Fig. 8.6 are the results of Lam et al. At a pump power of around $60 \pm 10\%$, they found an optimal vacuum squeezing of more than 7.0 ± 0.2 dB.

In some applications it is desirable to have a squeezed stater with a non zero coherent amplitude, a *bright* squeezed state. The conventional way to do this would be to simply mix the squeezed vacuum state produced by the OPO with a coherent state on a beam splitter (see Exercise 8.1). However the transmitivity of the squeezed vacuum state must be very close to unity in order not to loose the squeezing. This means that very little of the coherent light is reflected and the scheme is rather wasteful of power. Lam et al. also showed two alternative methods to produce a squeezed state with a significant coherent amplitude. In the first method a small seed coherent beam was injected into the back face of the OPO. This gave an amplitude squeezed state with 4 dB of squeezing. The second method was based on electro-optical feed-forward to transfer the squeezing onto a coherent beam, see Fig. 8.7. By carefully adjusting the gain on the controlling photon current to the EOM a bright squeezed beam with squeezing in the amplitude quadrature corresponding to a reduction of intensity noise of 4db below shot noise.

8.2 Twin Beam Generation and Intensity Correlations

Another second-order process which can produce non-classical states is non-degenerate down conversion. A pump photon with frequency 2ω creates a signal and an idler photon each with frequency ω but different polarisations.

Alternatively the signal and idler may be distinguished by having different frequencies ω_1 and ω_2, respectively, such that $\omega_1 + \omega_2 = 2\omega$. Such a process ensures that the photon numbers in the signal and idler beams are highly correlated. Although the intensity of each beam may fluctuate, the fluctuations on the two beams are identical. This suggests that the intensity difference of the two beams will carry no fluctuations at all. That is to say, the variance of $I_1 - I_2$ can be zero. If the process occurs inside a cavity the correlation between the two photons may be lost as photons escape the cavity. This is true for times short compared to the cavity lifetime. For long times, however, the correlation is restored; if one waits long enough all photons will exit the cavity. Consequently the spectrum of fluctuations in the difference of the intensities in the two beams reduces to zero at zero frequency.

The Hamiltonian describing this process may be written as

$$\mathscr{H}_I = \mathrm{i}\hbar\chi(a_0 a_1^\dagger a_2^\dagger - a_0^\dagger a_1 a_2)\,, \tag{8.23}$$

where a_0 describes the pump field, while a_1 and a_2 describe the signal and idler fields. The pump field is driven by a coherent field external to the cavity with amplitude ε. The damping rates for the three cavity modes a_0, a_1 and a_2 are κ_0, κ_1 and κ_2, respectively.

Following from the Fokker–Planck equation for the positive P representation we establish the c-number stochastic differential equations [6]

$$\begin{aligned}
\dot{\alpha}_0 &= -\kappa_0\alpha_0 + \varepsilon - \chi\alpha_1\alpha_2\,,\\
\dot{\alpha}_1 &= -\kappa_1\alpha_1 + \chi\alpha_0\alpha_2^\dagger + R_1(t)\,,\\
\dot{\alpha}_2 &= -\kappa_2\alpha_2 + \chi\alpha_0\alpha_1^\dagger + R_2(t)\,.
\end{aligned} \tag{8.24}$$

In our treatment we will assume for simplicity that $\kappa_1 = \kappa_2 = \kappa$, where the only non-zero noise correlation functions are

$$\begin{aligned}
\langle R_1(t)R_2(t')\rangle &= \chi\langle\alpha_0\rangle\delta(t-t'),\\
\langle R_1^\dagger(t)R_2^\dagger(t')\rangle &= \chi\langle\alpha_0^\dagger\rangle\delta(t-t')\,.
\end{aligned} \tag{8.25}$$

The semi-classical steady state solutions depend on whether the driving field ε is above or below a critical "threshold" value given by

$$\varepsilon_{\mathrm{thr}} = \frac{\kappa_0\kappa}{\chi}\,. \tag{8.26}$$

Above threshold one of the eigenvalues of the drift matrix is zero. This is associated with a phase instability. To see this we use an amplitude and phase representation:

$$\alpha_j(t) = r_j[1+\mu_j(t)]\mathrm{e}^{-\mathrm{i}(\phi_j+\psi_j(t))} \tag{8.27}$$

where r_j, ϕ_j are the steady state solutions, and $\mu_j(t)$ and $\psi_j(t)$ represent small fluctuations around the steady state. Solving for the steady state below threshold we have

$$r_1 = r_2 = 0, \qquad r_0 = \frac{|\varepsilon|}{\kappa_0}\,, \qquad \phi_0 = \phi_{\rm p}\,, \tag{8.28}$$

where we have used $\varepsilon = |\varepsilon| e^{i\phi_{\rm p}}$, with $\phi_{\rm p}$ denoting the phase of the coherent pump. Above threshold

$$\begin{aligned} r_0 &= \frac{\kappa}{\chi}, \quad \phi_0 = \phi_{\rm p}\,, \\ r_1 = r_2 &= \frac{\sqrt{\kappa_0}\kappa}{\chi}(E-1)^{1/2}\,, \qquad \phi_1 + \phi_2 = \phi_{\rm p}\,, \end{aligned} \tag{8.29}$$

with

$$E = \frac{|\varepsilon|}{|\varepsilon_{\rm thr}|}\,. \tag{8.30}$$

Note that in the above threshold solution only the sum of the signal and idler phases is defined. No steady state exists for the phase difference. It is the phase difference variable which is associated with the zero eigenvalue.

We now turn to an analysis of the intensity fluctuations above threshold. The nonlinear dynamics of (8.24) is approximated by a linear dynamics for intensity fluctuations about the steady states above threshold. Define the new variables by

$$\Delta I_j = \alpha_j^\dagger \alpha_j - I_j^{\rm ss}\,, \tag{8.31}$$

where $I_j^{\rm ss}$ is the steady state intensity above threshold for each of the three modes. It is more convenient to work with scaled "intensity-sum" and 'intensity-difference' variables defined by

$$\Delta I_{\rm s} = \kappa(\Delta I_1 + \Delta I_2), \qquad \Delta I_{\rm D} = \kappa(\Delta I_1 - \Delta I_2)\,, \tag{8.32}$$

The linear stochastic differential equations are then given by

$$\Delta \dot{I}_0 = -\kappa_0 \Delta I_0 - \Delta I_{\rm s}\,, \tag{8.33}$$

$$\Delta \dot{I}_{\rm s} = 2\kappa\kappa_0(E-1)\Delta I_0 + F_{\rm s}(t)\,, \tag{8.34}$$

$$\Delta \dot{I}_{\rm D} = -2\kappa \Delta I_{\rm D} + F_{\rm D}(t)\,, \tag{8.35}$$

where the non zero noise correlations are

$$\langle F_{\rm s}(t) F_{\rm s}(t')\rangle = -\langle F_{\rm D}(t) F_{\rm D}(t')\rangle = 4\frac{\kappa_0\kappa^4}{\chi^2}(E-1)\delta(t-t')\,. \tag{8.36}$$

We are now in a position to calculate the spectrum of fluctuations in the intensity difference in the signal and idler modes outside the cavity. The equation for the intensity difference fluctuations may be solved immediately to give

$$\Delta I_0(t) = \Delta I_{\rm D}(0) e^{-2\kappa t} + \int_0^t {\rm d}t' e^{-2\kappa(t-t')} F_{\rm D}(t')\,. \tag{8.37}$$

Thus the steady state two-time correlation function is found to be

$$\langle I_{\rm D}(\tau)\ ,\ I_{\rm D}(0)\rangle = \langle \Delta I_{\rm D}(\tau)\Delta I_{\rm D}(0)\rangle = \frac{\kappa_0\kappa^3}{\chi^2}(E-1)\mathrm{e}^{-2\kappa\tau} \tag{8.38}$$

with $\langle A,B\rangle = \langle AB\rangle - \langle A\rangle\langle B\rangle$.

The spectrum of fluctuations in the intensity difference field outside the cavity is defined by

$$S_{\rm D}(\omega) = \int \mathrm{d}\tau \mathrm{e}^{-\mathrm{i}\omega\tau}\langle \hat{I}_1(\tau) - \hat{I}_2(\tau), \hat{I}_1(0) - \hat{I}_2(0)\rangle_{\rm ss}\ , \tag{8.39}$$

where $\hat{I}_j(t)$ are the external intensity operators. However, from Chap. 7, we can relate this operator average to the c-number averages for $\alpha_j(t)$ inside the cavity. The result is

$$\langle \hat{I}_j(\tau),\ \hat{I}_k(0)\rangle = 2\delta_{jk}\kappa\delta(\tau)\langle I_j(0)\rangle + 4\kappa^2\langle I_j(\tau),\ I_k(0)\rangle\ , \tag{8.40}$$

where $I_j \equiv \alpha_j^\dagger(t)\alpha_j(t)$. Finally, we write the result directly in terms of the valuables $\Delta I_{\rm D}(t)$,

$$S_{\rm D}(\omega) = S_0 + 4\int \mathrm{d}\tau \mathrm{e}^{-\mathrm{i}\omega\tau}\langle \Delta I_{\rm D}(\tau)\Delta I_{\rm D}(0)\rangle\ , \tag{8.41}$$

where

$$S_0 = 2\kappa(\langle I_1\rangle_{\rm ss} + \langle I_2\rangle_{\rm ss}) = \frac{4\kappa_0\kappa^3}{\chi^2}(E-1)\ . \tag{8.42}$$

The frequency independent term S_0 represents the contribution of the shot-noise from each beam. Thus to quantify the degree of reduction below the shot-noise level we define the 'normalised' intensity difference spectrum

$$\bar{S}_{\rm D}(\omega) \equiv \frac{S_{\rm D}(\omega)}{S_0}\ . \tag{8.43}$$

Substituting (8.38 and 8.42) into (8.41), and integrating we obtain

$$\bar{S}_{\rm D}(\omega) \equiv \frac{\omega^2}{\omega^2 + 4\kappa^2}\ . \tag{8.44}$$

This is a simple inverted Lorentzian with a width 2κ. As expected, at zero frequency there is perfect noise suppression in the intensity difference between the signal and idler. This result was first obtained by *Reynaud* et al. [7].

The above results assume no additional cavity losses beyond those corresponding to the (equal) transmitivities at the output mirror. When additional losses are included the correlation between the signal and idler is no longer perfect as one of the pair of photons may be lost otherwise than through the output mirror. In that case there is no longer perfect suppression of quantum noise at zero frequency [8]. The result is shown in Fig. 8.8a. Furthermore, the spectrum of intensity difference fluctuations is very sensitive to any asymmetry in the loss for each mode [8]. In Fig. 8.8b we depict the effect of introducing different intracavity absorption rates

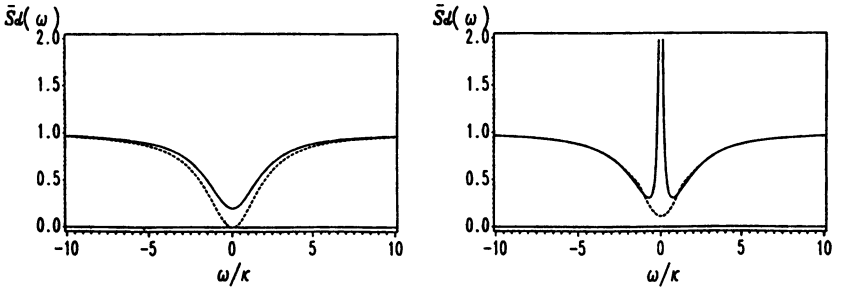

Fig. 8.8 The effect of intracavity absorption on the intensity difference spectrum. (**a**) A plot of the normalized spectrum when the total cavity losses for each mode are equal to the total loss from the pump mode, and greater than the output loss rate κ (*solid line*). The dashed line shows the perfect case when the only losses are through the output mirrors. (**b**) The effect of asymmetrical intracavity absorption. The total loss for the idler is equal to the idler damping rate but the damping rate for the signal is only 80% of the total loss for that mode. $E = 1.05$ solid line, $E = 2.0$, dashed line. [8]

for each mode. This phenomenon could form the basis of a sub-shot-noise absorption spectrometer.

The prediction of noise suppression in the differenced intensity has been confirmed in the experiment of *Heidmann* et al. [9]. They used a type II phase-matched potassium triphosphate, known as KTP, crystal placed inside an optical cavity, thus forming an Optical Parametric Oscillator (OPO).

The damping constant at the pump frequency was much greater than for the signal and idler. Above threshold the OPO emits two cross polarised twin beams at approximately the same frequency. The twin beams are separated by polarising beam splitters and then focussed on two photodiodes which have quantum efficiencies of 90%. The two photo-currents are amplified and then subtracted with a 180° power combiner. The noise on the resulting difference current is then monitored by a spectrum analyser.

A maximum noise reduction of $30\% \pm 5\%$ is observed at a frequency of 8 MHz. The noise reduction is better than 15% from 3 to 13 MHz. The noise reduction is limited due to other losses inside the OPO and various detector inefficiencies.

Using an α-cut KTP crystal, *Gao* et al. [10] achieved a noise reduction in the intensity difference of 88% below the shot noise level, corresponding to a 9.2 dB reduction. They also showed how such highly correlated intensities could be used to enhance the signal-to-noise ratio for relative absorption measurements when one beam passes through an absorber. The improvement was about 7 dB.

The bandwidth of squeezing in cavity experiments is restricted to the cavity bandwidth. Single-pass experiments are feasible using the higher intensity possible with pulsed light. Pulsed twin beams of light have been generated by means of an optical parametric amplifier that is pumped by the second harmonic of a mode-locked and Q-switched Nd : YAG laser [11]. While the noise levels of the individual signal and idler beams exceed their coherent state limits by about 11 dB the correlation is so strong that the noise in the difference current falls below the quantum limit by more than 6 dB (75%).

8.2.1 Second Harmonic Generation

We now consider second harmonic generation setting $E_2 = 0$. For both the second harmonic and fundamental modes the squeezing increases monotonically as $|\varepsilon_2|$ increases from zero to the critical value $|\varepsilon_2| = \gamma_1 + \gamma_2$. The squeezing spectrum splits into two peaks first for the fundamental and then provided $\gamma_2^2 > \frac{1}{2}\gamma_1^2$ for the second harmonic.

Above the critical point the system exhibits self-sustained oscillations. We plot the maximum squeezing as a function of the driving field E_1 for both the fundamental and second harmonic in Fig. 8.9 [3].

In both the cases considered the maximum squeezing occurs as an instability point is approached. This is an example of critical quantum fluctuations which are asymmetric in the two quadrature phases. It is clear that in order to approach zero fluctuations in one quadrature the fluctuations in the other must diverge. At the critical point itself, with the critical frequency being $\omega_c^2 = \gamma_2(\gamma_2 + 2\gamma_1)$ (which is, in fact, the initial frequency of the hard mode oscillations) we have for the amplitude quadrature of the fundamental.

$$S_{1+}^{\mathrm{OUT}}(\omega_c) = 1 - \frac{\gamma_1}{\gamma_1 + \gamma_2}\,, \tag{8.45}$$

which gives perfect squeezing for $\gamma_1 \gg \gamma_2$ at $\omega = \pm\sqrt{2\gamma_1\gamma_2}$, and for the amplitude quadrature of the second harmonic

$$S_{2+}^{\mathrm{OUT}}(\omega_c) = 1 - \frac{\gamma_2}{\gamma_1 + \gamma_2}\,, \tag{8.46}$$

this gives perfect squeezing for $\gamma_2 \gg \gamma_1$ at $\omega = \gamma_2$. The squeezing spectra for the two modes at the critical point is shown in Fig. 8.10. The fluctuations in the phase quadrature must tend to infinity, a characteristic of critical fluctuations. We note that the linearization procedure we have used will break down in the vicinity of the critical point and in practice the systems will operate some distance from the critical point.

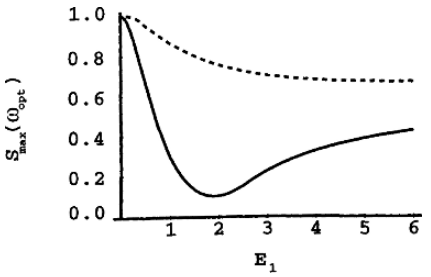

Fig. 8.9 A plot of the maximum squeezing versus driving field amplitude for second harmonic generation. The solid line is the fundamental, the dashed line is the second-harmonic. $\gamma_1 = \gamma_2 = 1.0$

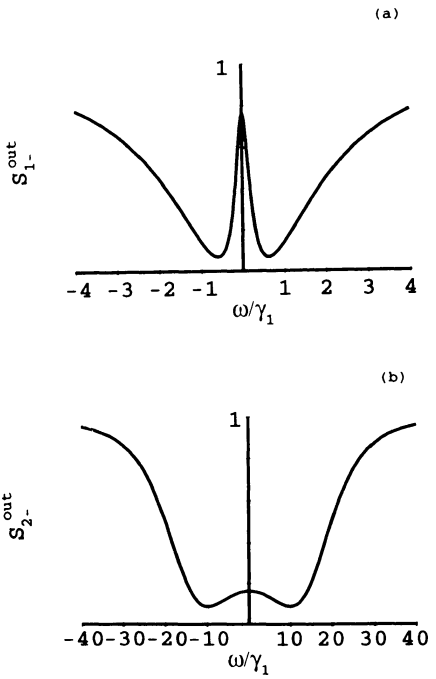

Fig. 8.10 The squeezing spectrum for the fundamental and the second harmonic at the critical point for oscillation. $\gamma_1 = 1.0$, (**a**) $\gamma_2 = 0.1$, (**b**) $= \gamma_2 = 10.0$

8.2.2 Experiments

The earliest experiments to demonstrate amplitude squeezing in second harmonic generation were done by *Pereira* et al. [12] and by *Sizman* et al. [13]. Both experiments used a crystal of MgO:$LiNbO_3$ and driven by a frequency stabilised Nd:Yag laser. In second harmonic generation the squeezing appears in the amplitude quadrature so a direct detection scheme can be employed. In the case of Pereira et al. the nonlinear crystal was inside an optical cavity. They looked for squeezing at the fundamental frequency. Sensitivity to phase noise in both the pump laser and from scattering processes in the crystal limited the observed squeezing to 13% reduction relative to vacuum. Sizman et al. used a monolithic crystal cavity. The end faces of the crystal have dielectric mirror coatings with a high reflectivity for both the fundamental and second harmonic modes. They reported a 40% reduction in the intensity fluctuations of the second harmonic light. These two schemes used a doubly resonant cavity, i.e. both the fundamental and the second harmonic are resonant with the cavity. This poses a number of technical difficulties not least of which is maintaining the double resonance condition for extended periods. *Paschotta* et al. [14] demonstrated a singly resonant cavity at the fundamental frequency for generating amplitude squeezed light in the second harmonic mode. Using a MgO:LiNbO3 monolithic standing-wave cavity they measured 30% noise reduction (1.5 dB) at 532 nm. The

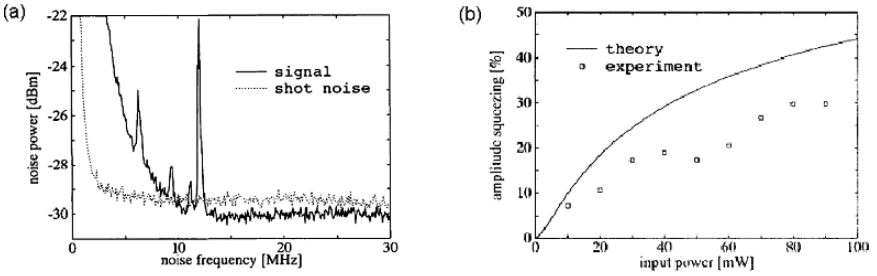

Fig. 8.11 (**a**) A typical noise spectrum. Squeezing is apparent above about 12 MHz. (**b**) Squeezing as percent of vacuum level at 16 MHz. The experimental results (*squares*) are corrected for known inefficiencies. From [14]

results of this experiment are shown in Fig. 8.11. *Tsuchida* et al. also demonstrated amplitude-squeezed light in the second harmonic mode at 431 nm in with a $KNbO_3$ crystal, in a singly resonant at the fundamental mode. Noise reduction of 2.4 dB at 7.5 MHz was observed in the second harmonic mode.

The purpose of a cavity is to enhance the pump power and get a sufficiently large nonlinear response. However it is possible to get squeezing without a cavity. *Serkland* et al. [15] demonstrated that traveling-wave second-harmonic generation produces amplitude-squeezed light at both the fundamental and the harmonic frequencies. The amplitude noise of the transmitted fundamental field was measured to be 0.8 dB below the shot-noise level, and the generated 0.765-mm harmonic light was measured to be amplitude squeezed by 0.35 dB. The conversion-efficiency dependence of the observed squeezing at both wavelengths agrees with theoretical predictions.

8.3 Applications of Squeezed Light

8.3.1 Interferometric Detection of Gravitational Radiation

Interest in the practical generation of squeezed states of light became significant when *Caves* [16] suggested in 1981 that such light might be used to achieve better sensitivity in the interferometric detection of gravitational radiation. The result of *Caves* indicated that while squeezed light would not increase the maximum sensitivity of the device, it would enable maximum sensitivity to be achieved at lower laser power. Later analyses [17, 18, 19, 20] demonstrated that by an optimum choice of the phase of the squeezing it is possible to increase the maximum sensitivity of the interferometer. This result was established by a full nonlinear quantum theory of the entire interferometer, including the action of the light pressure on the end mirrors. We shall demonstrate this following the treatment of *Pace* et al. [20].

A schematic illustration of a laser interferometer for the detection of gravitational radiation is shown in Fig. 8.12. To understand how the device works we need to

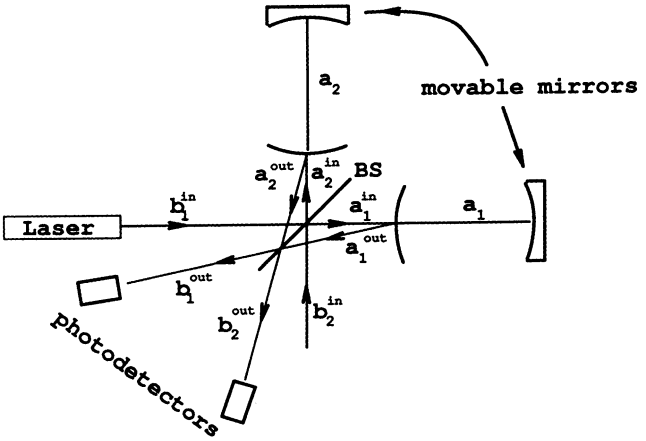

Fig. 8.12 Schematic representation of a laser interferometer for the detection of gravitational radiation

recall some properties of gravitational radiation. A gravitational wave induces weak tidal forces, in a plane perpendicular to the direction of propagation. A gravitational wave passing normal to a circular arrangement of masses would periodically force the circle into an ellipse [21]. In the case of the interferometer depicted in Fig. 8.12, the end mirrors of the two cavities are constrained by a weak harmonic potential, and lie on a circular arc separated by 90°. Thus, when a gravitational wave passes orthogonal to the plane of the interferometer, one cavity will be shortened as the other cavity is lengthened. If the intensity difference of the light leaving each arm of the interferometer is monitored, the asymmetric detuning of each cavity caused by the moving end mirrors causes this intensity to be modulated at the frequency of the gravitational wave.

While this scheme sounds very promising it suffers from a big problem. Even though gravitational radiation reaching terrestrial detectors is highly classical (many quanta of excitation) it interacts very weakly with the end mirrors. The relative change in the length of each cavity is then so small that it is easily lost amid a multitude of noise sources, which must somehow be reduced if any systematic effect is to be observed. To begin with, it is necessary to isolate the end mirrors from external vibrations and seismic forces. Then one must ensure that the random thermal motion of the end mirrors is negligible. Ultimately as each end mirror is essentially an oscillator, there is the zero-point motion to take account of. Quite apart from the intrinsic noise in the motion of the end mirrors, noise due to the light also limits the sensitivity of the device. The light noise can be separated into two contributions. Firstly the measurement we ultimately perform is an intensity measurement which is limited by shot-noise. In the case of shot-noise, however, the signal-to-noise ratio scales as the square root of the input power, thus one might attempt to avoid this noise source by simply raising the input power. Unfortunately, increasing the input power increases the contribution from another source – radiation

pressure. Individual photons reflecting from the end mirrors cause a random force large enough to mask the very small movements due to gravitational radiation.

In the light of the above discussion it would seem that trying to detect gravitational radiation in this manner will be hopeless. However, as we now show, a careful study reveals that while the task is difficult it is achievable and made more so by the careful use of squeezed light. In this calculation we treat each end mirror as a damped simple harmonic oscillator subject to zero-point fluctuations and the classical driving force of the gravitational wave. Thus we assume the thermal motion has been eliminated. We also include the radiation pressure force and associated fluctuations in the cavity fields.

To begin we first determine how the intracavity fields determine the intensity difference signal. Denote the intracavities fields by the annihilation operators a_i $(i = 1,\ 2)$ and the input and output fields for each cavity are represented by $a_i^{\rm in}$ and $a_i^{\rm out}$, respectively. Let $b_i^{\rm in}$ and $b_i^{\rm out}$ denote the input and output fields for each arm of the interferometer. The central beam-splitter (BS in Fig. 8.12) connects the cavity inputs and outputs to the interferometer inputs and outputs by

$$a_1^{\rm in} = \frac{1}{\sqrt{2}}(b_1^{\rm in} + {\rm i}b_2^{\rm in})\,, \tag{8.47}$$

$$a_2^{\rm in} = \frac{1}{\sqrt{2}}(b_1^{\rm in} + {\rm i}b_2^{\rm in})\,, \tag{8.48}$$

$$b_1^{\rm out} = \frac{1}{\sqrt{2}}(a_1^{\rm out} + {\rm i}a_2^{\rm out}{\rm e}^{{\rm i}\phi})\,, \tag{8.49}$$

$$b_2^{\rm out} = \frac{1}{\sqrt{2}}(a_1^{\rm out} + {\rm i}a_2^{\rm out}{\rm e}^{{\rm i}\phi})\,, \tag{8.50}$$

where ϕ is a controlled phase shift inserted in arm 2 of the interferometer to enable the dc contribution to the output intensity difference to be eliminated.

The measured signal is then represented by the operator

$$\begin{aligned} I_-(t) &= (b_1^{\rm out})^\dagger b_1^{\rm out} - (b_2^{\rm out})^\dagger b_2^{\rm out} \\ &= -{\rm i}[(a_2^{\rm out})^\dagger a_1^{\rm out}{\rm e}^{-{\rm i}\phi} - {\rm h.c.}]\,. \end{aligned} \tag{8.51}$$

Now the relationship between the cavity fields and the respective input and output fields is given by

$$a_{\rm i}^{\rm out} = \sqrt{\gamma}a_{\rm i} - a_{\rm i}^{\rm in} \quad (i = 1,\ 2)\,, \tag{8.52}$$

where we assume the damping rate for each cavity, γ, is the same.

We now assume that arm one of the interferometer is driven by a classical coherent source with amplitude $E/\sqrt{\gamma}$ in units such that the intensity of the input is measured in photons/second. The scaling $\gamma^{-1/2}$ is introduced, for convenience. Then from (8.47 and 8.48), each cavity is driven with the same amplitude $\varepsilon/\sqrt{\gamma}$, where $\varepsilon = E/\sqrt{2}$. That is

$$\langle a_1^{\rm in}\rangle = \langle a_2^{\rm in}\rangle = \frac{\varepsilon}{\sqrt{\gamma}}\,. \tag{8.53}$$

As we show below, it is possible to operate the device in such a way that in the absence of gravitational radiation, a stable deterministic steady state amplitude α_0 is established in each cavity. This steady state is then randomly modulated by fluctuations in the cavity fields and deterministically modulated by the moving end mirrors of each cavity. Both these effects are of similar magnitude. It thus becomes possible to linearise the output fields around the stationary states. With this in mind we now define the fluctuation operators δa_i and $\delta a_i^{\rm in}$ for each cavity $(i = 1,\ 2)$

$$\delta a_i = a_i - \alpha_0 \,, \tag{8.54}$$

$$\delta a_i^{\rm in} = a_i^{\rm in} - \frac{\varepsilon}{\sqrt{\gamma}} \,. \tag{8.55}$$

Using these definitions, together with (8.47–8.50), in (8.51), the output signal is then described by the operator

$$I_-(t) = \frac{\gamma\alpha_0}{2}[\delta y_1(t) - \delta y_2(t)] - \frac{\sqrt{\gamma}\alpha_0}{2}[\delta y_1^{\rm in}(t) - \delta y_2^{\rm in}(t)] \,, \tag{8.56}$$

where

$$\delta y_i(t) \equiv {\rm i}(\delta a_i - \delta a_i^\dagger) \,, \tag{8.57}$$

$$\delta y_i^{\rm in}(t) \equiv -{\rm i}[\delta a_{\rm i}^{\rm in} - (\delta a_{\rm i}^{\rm in})^\dagger] \,. \tag{8.58}$$

We have chosen the arbitrary phase reference so that the input amplitude, and thus the steady state amplitude α_0, is real.

Equation (8.56) indicates that the signal is carried by the phase quadrature not the amplitude quadrature. Thus we must determine $y_i(t)$.

We turn now to a description of the intracavity dynamics. The end mirror is treated as a quantised simple harmonic oscillator with position and momentum operators $(Q,\ P)$. The radiation pressure force is proportional to the intracavity photon number. The total Hamiltonian for the system may then be written [20]

$$\mathscr{H} = \hbar\Delta a^\dagger a + \frac{P^2}{2M} + \frac{M\Omega^2}{2}Q^2 - \hbar\frac{\omega_0}{L}a^\dagger aQ + F(t)Q \,, \tag{8.59}$$

where M is the mass of the end mirror, Ω is the oscillator frequency of the end mirror, L is the cavity length, Δ is the cavity detuning, and $F(t)$ is the driving force on the end mirror due to the gravitational wave. If we assume the acceleration produced by the gravitational wave is

$$g(t) = g\ \cos(\omega_{\rm g} t) \,, \tag{8.60}$$

the force $F(t)$ may be written as

$$F(t) = -MhL\omega_{\rm g}^2 S(t) \tag{8.61}$$

where h is defined to be the maximum fractional change in the cavity length, L, produced by the gravitational wave in the absence of all other forces, and $s(t) = {\rm co}(\omega_{\rm g} t)$.

It is convenient to define the dimensionless position q and the momentum variables p for the mirror, which are the analogue of the quadrature phase operators for the field,

$$q = \left(\frac{2\hbar}{M\Omega}\right)^{1/2} Q\,, \tag{8.62}$$

$$p = (2\hbar M\Omega)^{-1/2} P\,. \tag{8.63}$$

The commutation relations for these new variables is $[q,\ p] = \mathrm{i}/2$. Thus in the ground state, the variance in q and p are both equal to 1/4.

The quantum stochastic differential equations for this system may now be written

$$\frac{\mathrm{d}a}{\mathrm{d}t} = \varepsilon - \mathrm{i}(\Delta + 2\kappa q)a - \frac{\gamma}{2}a + \sqrt{\gamma}a^{\mathrm{in}}\,, \tag{8.64}$$

$$\frac{\mathrm{d}q}{\mathrm{d}t} = \Omega p - \frac{\Gamma}{2}q + \sqrt{\Gamma}q^{\mathrm{in}}\,, \tag{8.65}$$

$$\frac{\mathrm{d}p}{\mathrm{d}t} = -\Omega q - \kappa a^{\dagger}a - \kappa s(t) - \frac{\Gamma}{2}p + \sqrt{\Gamma}p^{\mathrm{in}}\,, \tag{8.66}$$

where

$$\kappa \equiv \frac{-\omega_0}{L}\left(\frac{\hbar}{2M\Omega}\right)^{1/2}\,, \tag{8.67}$$

$$k = -hL\omega_{\mathrm{g}}^2\left(\frac{M}{2\hbar\Omega}\right)^{1/2}\,, \tag{8.68}$$

and $\gamma/2$ is the damping rate for the intracavity field, while $\Gamma/2$ is the damping rate for the end mirrors. Note that the form of the stochastic equation for the mirror is that for a zero-temperature, under-damped oscillator and will thus only be valid provided $\Gamma \ll \Omega$.

Let us first consider the corresponding deterministic semi-classical equations

$$\dot{\alpha} = \varepsilon - \mathrm{i}(\Delta + 2\kappa q)\alpha - \frac{\gamma}{2}\alpha\,, \tag{8.69}$$

$$\dot{q} = \Omega p - \frac{\Gamma}{2}q\,, \tag{8.70}$$

$$\dot{p} = -\Omega q - \kappa|\alpha|^2 - ks(t) - \frac{\Gamma}{2}p\,. \tag{8.71}$$

These equations represent a pair of nonlinearly coupled harmonically driven oscillators, and as such are candidates for unstable, chaotic behaviour. However, the amplitude of the driving, k, is so small that one expects the system to remain very close to the steady state in the absence of driving. The first step is thus to determine the steady state values, $\alpha_0,\ q_0$ and p_0. If we choose Δ such that $\Delta = -2\kappa q_0$ (so the cavity is always on resonance), then

$$\alpha_0 = \frac{2\varepsilon}{\gamma} \,. \tag{8.72}$$

Of course, this steady state itself may be unstable. To check this we linearise the undriven dynamics around the steady state. Define the variables

$$\delta x(t) = \mathrm{Re}\{\alpha(t) - \alpha_0\} \,, \tag{8.73}$$
$$\delta y(t) = \mathrm{Im}\{\alpha(t) - \alpha_0\} \,, \tag{8.74}$$
$$\delta q(t) = q(t) - q_0 \,, \tag{8.75}$$
$$\delta p(t) = p(t) - p_0 \,. \tag{8.76}$$

Then

$$\frac{\mathrm{d}}{\mathrm{d}t}\begin{pmatrix}\delta x\\ \delta y\\ \delta q\\ \delta p\end{pmatrix} = \begin{pmatrix}-\frac{\gamma}{2} & 0 & 0 & 0\\ 0 & -\frac{\gamma}{2} & -\mu & 0\\ 0 & 0 & -\frac{\Gamma}{2} & \Omega\\ -\mu & 0 & -\Omega & -\frac{\Gamma}{2}\end{pmatrix}\begin{pmatrix}\delta x\\ \delta y\\ \delta q\\ \delta p\end{pmatrix} \,, \tag{8.77}$$

where $\mu = 4\kappa\alpha_0$ and we have assumed ε and thus α_0 are real. The eigenvalues of the linear dynamics are then found to be $(-\gamma/2,\ -\gamma/2,\ -\Gamma/2 + \mathrm{i}\Omega,\ -\Gamma/2 - \mathrm{i}\Omega)$, so clearly the steady state is stable in the absence of the gravitational wave.

We shall point out the interesting features of (8.77). First we note that the quadrature carrying the coherent excitation (δx) is totally isolated from all other variables. Thus $\delta x(t) = \delta x(0)\mathrm{e}^{-\gamma t/2}$. However, as fluctuations evolve from the steady state $\delta x(0) = 0$, one can completely neglect the variables $\delta x(t)$ for the deterministic part of the motion. Secondly we note the mirror position fluctuations δq feed directly into the field variable $\delta y(t)$ and thus directly determine the output intensity difference signal by (8.56). Finally, we note the fluctuations of the in-phase field variable δx drive the fluctuating momentum of the mirror. This is, of course, the radiation pressure contribution. However, for the deterministic part of the dynamics $\delta x(t) = 0$, as discussed above, so the mirror dynamics is especially simple – a damped harmonic oscillator. In the presence of the gravitational wave the deterministic dynamics for the end mirrors is then

$$\begin{pmatrix}\delta\dot{q}\\ \delta\dot{p}\end{pmatrix} = \begin{pmatrix}-\frac{\Gamma}{2} & \Omega\\ -\Omega & -\frac{\Gamma}{2}\end{pmatrix}\begin{pmatrix}\delta q\\ \delta p\end{pmatrix} - \begin{pmatrix}0\\ ks(t)\end{pmatrix} \,, \tag{8.78}$$

with the initial conditions $\delta q(0) = \delta p(0)$ the solution for $\delta q(t)$ is

$$\delta q(t) = R\,\cos(\omega_{\mathrm{g}} t + \phi) \,, \tag{8.79}$$

with

$$R = \frac{k\Omega}{\left|\frac{\Gamma}{2} + \mathrm{i}(\omega_{\mathrm{g}} - \Omega)\right|\left|\frac{\Gamma}{2} + \mathrm{i}(\omega_{\mathrm{g}} + \Omega)\right|} \,, \tag{8.80}$$

$$\phi = \arctan\left(\frac{-\Gamma\omega_{\mathrm{g}}}{\frac{\Gamma^2}{4} + \Omega^2 - \omega_{\mathrm{g}}^2}\right) \,. \tag{8.81}$$

Substituting this solution into the equation for $\delta y(t)$ and solving, again with $\delta y(0) = 0$, we find

$$\delta y(t) = \frac{-4\kappa\alpha_0 R}{\left|\frac{\gamma}{2} + \mathrm{i}\omega_\mathrm{g}\right|} \cos(\omega_\mathrm{g} t + \theta + \phi) \,, \tag{8.82}$$

where

$$\theta = \arctan\left(\frac{\alpha\omega_\mathrm{g}}{\gamma}\right) . \tag{8.83}$$

We have neglected an initial decaying transient. Apart from the phase shifts θ and ϕ, the out-of-phase field quadrature follows the displacements of the end mirror induced by the gravitational wave.

Due to the tidal nature of the gravitational wave if one cavity end mirror experiences a force $F(t)$, the other experiences $-F(t)$. Thus $\delta y_1(t) = -\delta y_2(t)$ and the mean signal is

$$\langle I_-(t)\rangle = -\frac{16\kappa I R \cos(\omega_\mathrm{g} t + \phi + \theta)}{\left|\frac{\gamma}{2} + \mathrm{i}\omega_\mathrm{g}\right|} \,, \tag{8.84}$$

where the output intensity I is defined by

$$I = |\langle a_i^{\mathrm{out}}\rangle|^2 = \frac{\gamma\alpha_0^2}{4} \,. \tag{8.85}$$

Using the definitions in (8.80, 8.67 and 8.68) we find

$$\langle I_-(t)\rangle = \frac{-8hI\omega_0\omega_\mathrm{g}^2 \cos(\omega_\mathrm{g} t + \theta + \phi)}{\left|\frac{\gamma}{2} + \mathrm{i}\omega_\mathrm{g}\right| \left|\frac{\Gamma}{2} + \mathrm{i}(\omega_\mathrm{g} - \Omega)\right| \left|\frac{\Gamma}{2} + \mathrm{i}(\omega_\mathrm{g} + \Omega)\right|} \tag{8.86}$$

and the signal is directly proportional to the mirror displacement h.

Before we consider a noise analysis of the interferometer it is instructive to look at the frequency components of variable $\delta y(t)$ by

$$\delta y(\omega) = \int_{-\infty}^{\infty} \mathrm{d}t \; \mathrm{e}^{\mathrm{i}\omega t} \, \delta y(t) \,. \tag{8.87}$$

As $\delta y(t)$ is real we have that $\delta y(t) = \delta y^*(-\omega)$. This relationship enables us to write

$$\delta y(t) = \int_0^{\infty} \mathrm{d}\omega [\delta y(\omega) \mathrm{e}^{-\mathrm{i}\omega t} + \delta y(\omega)^* \mathrm{e}^{\mathrm{i}\omega t}] \,, \tag{8.88}$$

thus distinguishing positive and negative frequency components. Inspection of (8.84) immediately gives that

$$\delta y(\omega) = \frac{-2\kappa\alpha_0 R \mathrm{e}^{-\mathrm{i}(\theta+\phi)}}{\left|\frac{\gamma}{2} + \mathrm{i}\omega_\mathrm{g}\right|} \delta(\omega - \omega_\mathrm{g}) \,. \tag{8.89}$$

Thus

$$|\langle I_-(\omega)\rangle| = hS(\omega_\mathrm{g})\delta(\omega - \omega_\mathrm{g}) \,, \tag{8.90}$$

where

$$S(\omega_{\rm g}) = \frac{8hI\omega_0\omega_{\rm g}^2}{\left|\frac{\gamma}{2}+{\rm i}\omega_{\rm g}\right|\left|\frac{\Gamma}{2}+{\rm i}(\omega_{\rm g}-\omega)\right|\left|\frac{\Gamma}{2}+{\rm i}(\omega_{\rm g}+\Omega)\right|}\,. \tag{8.91}$$

We now analyse the noise response of the interferometer. As the gravitational wave provides an entirely classical driving of the mirrors it can only effect the deterministic part of the dynamics, which we have already described above. To analyse the noise component we must consider the fluctuation *operators* δx, δy, δq and δp defined by $\delta x = x(t) - x_{\rm s}(t)$, where $x_{\rm s}$ is the semi-classical solution. In this way the deterministic contribution is removed.

The quantum stochastic differential equations are then

$$\frac{\rm d}{{\rm d}t}\delta x(t) = -\frac{\gamma}{2}\delta x(t) + \sqrt{\gamma}\delta x^{\rm in}(t)\,, \tag{8.92}$$

$$\frac{\rm d}{{\rm d}t}\delta y(t) = -\frac{\gamma}{2}\delta y(t) - \mu\,\delta q(t) + \sqrt{\gamma}\delta y^{\rm in}(t)\,, \tag{8.93}$$

$$\frac{\rm d}{{\rm d}t}q(t) = -\frac{\Gamma}{2}q(t) + \Omega p(t) + \sqrt{\Gamma}q^{\rm in}(t)\,, \tag{8.94}$$

$$\frac{\rm d}{{\rm d}t}p(t) = -\frac{\Gamma}{2}p(t) - \Omega q(t) - \mu x(t) + \sqrt{\Gamma}p^{\rm in}(t)\,, \tag{8.95}$$

with the only non-zero noise correlations being

$$\langle \delta x^{\rm in}(t)\delta x^{\rm in}(t')\rangle = \langle \delta y^{\rm in}(t)\delta y^{\rm in}(t')\rangle = \delta(t-t')\,, \tag{8.96}$$

$$\langle \delta x^{\rm in}(t)\delta y^{\rm in}(t')\rangle = \langle \delta y^{\rm in}(t)\delta x^{\rm in}(t')\rangle^* = {\rm i}\delta(t-t')\,, \tag{8.97}$$

$$\langle q^{\rm in}(t)q^{\rm in}(t')\rangle = \langle p^{\rm in}(t)p^{\rm in}(t')\rangle = \delta(t-t')\,, \tag{8.98}$$

$$\langle q^{\rm in}(t)p^{\rm in}(t')\rangle = \langle p^{\rm in}(t)q^{\rm in}(t')\rangle^* = {\rm i}\delta(t-t')\,, \tag{8.99}$$

From an experimental perspective the noise response in the frequency domain is more useful. Thus we define

$$\delta y(\omega) = \int_{-\infty}^{\infty} {\rm d}t\ {\rm e}^{{\rm i}\omega t}\,\delta y(t) \tag{8.100}$$

and similar expressions for the other variables. As $\delta y(t)$ is Hermitian we have $\delta y(\omega) = \delta y(-\omega)^\dagger$. The two time correlation functions for the variables are then determined by

$$\langle \delta y(t)\delta y(0)\rangle = \int_{-\infty}^{\infty} {\rm d}\omega {\rm e}^{-{\rm i}\omega t}\langle \delta y(\omega)\delta y^\dagger(\omega)\rangle \tag{8.101}$$

and similar expressions for the other quantities. Thus our objective is to calculate the signal variance

$$V_{I_-}(\omega) = \langle I_-(\omega)I_-(\omega)^\dagger\rangle\,. \tag{8.102}$$

In order to reproduce the δ-correlated noise terms of (8.96–8.99), the correlation function in the frequency domain must be

$$\langle \delta x^{\rm in}(\omega)\delta x^{\rm in}(\omega')^\dagger\rangle = \langle \delta y^{\rm in}(\omega)\delta y^{\rm in}(\omega')\rangle = \delta(\omega-\omega')\,, \tag{8.103}$$

$$\langle \delta x^{\rm in}(\omega)\delta y^{\rm in}(\omega')^\dagger\rangle = \langle \delta y^{\rm in}(\omega)\delta x^{\rm in}(\omega')^\dagger\rangle^* = {\rm i}\delta(\omega-\omega')\,, \tag{8.104}$$

$$\langle q^{\rm in}(\omega)q^{\rm in}(\omega')^\dagger\rangle = \langle p^{\rm in}(\omega)p^{\rm in}(\omega')^\dagger\rangle = \delta(\omega-\omega')\,, \tag{8.105}$$

$$\langle q^{\rm in}(\omega)p^{\rm in}(\omega')^\dagger\rangle = \langle p^{\rm in}(\omega)q^{\rm in}(\omega')^\dagger\rangle^* = {\rm i}\delta(\omega-\omega')\,, \tag{8.106}$$

We now directy transform the equations of motion and solve the resulting algebraic equations for the frequency components. The result for the crucial field variable is

$$\delta y(\omega) = A\delta x^{\rm in}(\omega) + B\delta y^{\rm in}(\omega) + C_q{}^{\rm in}(\omega) + D_p{}^{\rm in}(\omega)\,, \tag{8.107}$$

where

$$\begin{aligned} A &= \frac{\mu^2\Omega\sqrt{\gamma}}{\Lambda(\omega)\left(\frac{\gamma}{2}-{\rm i}\omega\right)}, \\ B &= \frac{\sqrt{\gamma}}{\frac{\gamma}{2}-{\rm i}\omega}, \\ C &= \frac{-\mu\sqrt{\Gamma}\left(\frac{\Gamma}{2}-{\rm i}\omega\right)}{\Lambda(\omega)\left(\frac{\gamma}{2}-{\rm i}\omega\right)}, \\ D &= \frac{-\mu\sqrt{\Gamma}\Omega}{\Lambda(\omega)\left(\frac{\gamma}{2}-{\rm i}\omega\right)}\,. \end{aligned} \tag{8.108}$$

$$\Lambda(\omega) = \left(\frac{\Gamma}{2}-{\rm i}\omega\right)^2 + \Omega^2\,. \tag{8.109}$$

Thus

$$\begin{aligned} \langle y(\omega)y^\dagger(\omega)\rangle = {} & |A|^2\langle \delta x^{\rm in}(\omega)\delta x^{\rm in}(\omega)^\dagger\rangle + |B|^2\langle \delta y^{\rm in}(\omega)\delta y^{\rm in}(\omega)^\dagger\rangle \\ & + |C|^2\langle q^{\rm in}(\omega)q^{\rm in}(\omega)^\dagger\rangle + |D|^2\langle p^{\rm in}(\omega)p^{\rm in}(\omega')\rangle \\ & + (AB^*\langle \delta x^{\rm in}(\omega)\delta y^{\rm in}(\omega)^\dagger\rangle + {\rm c.c.}) \\ & + (CD^*\langle q^{\rm in}(\omega)p^{\rm in}(\omega)^\dagger\rangle + {\rm c.c.}) \end{aligned} \tag{8.110}$$

It is now constructive to consider the physical interpretation of each term. The first term proportional to the in-phase field amplitude is the error in the output intensity due to radiation pressure fluctuations. The second term is the error due to the out-of-phase amplitude of the field, i.e. the intrinsic phase fluctuations. The second and third terms are the fluctuations in mirror position and momentum due to intrinsic mirror fluctuations and radiation pressure. The fourth term represents correlations between the amplitude and the phase of the field due to radiation pressure modulating the length of the cavity. In a similar way the final term is the correlation

between the position and momentum of the mirror as the radiation pressure changes the momentum which is coupled back to the position under free evolution.

Define the normalised variance by

$$N(\omega) = \frac{V_{I-}(\omega)}{2I}\,, \tag{8.111}$$

where I is the output intensity from each cavity. This quantity is given by

$$N(\omega) = 1 + \frac{16\kappa^2 I\Gamma\left(\frac{\Gamma^2}{4} + \Omega^2 + \omega^2\right)}{|\Lambda(\omega)|^2\left|\frac{\gamma}{2} - \mathrm{i}\omega\right|^2} + \frac{(16\kappa^2 I)^2\Omega^2}{|\Lambda(\omega)|^2\left|\frac{\gamma}{2} - \mathrm{i}\omega\right|^4}\,. \tag{8.112}$$

The first term in (8.112) is the shot-noise of the incident light on the detector, the second term arises from the intrinsic (zero-point) fluctuations in the positions of the end mirrors, while the last term represents the radiation pressure noise.

In Fig. 8.13 we display the total noise $N(\omega)$ as a function of frequency (a) (solid line) together with the contributions to the noise from: (b) photon-counting noise (dashed line); (c) mirror noise (dash-dot line); (d) radiation-pressure noise (dotted line). Typical interferometer parameters, summarised in Table 8.1 were used.

From signal processing theory, a measurement at frequency ω_{g} of duration τ entails an error Δh in the displacement h given by

$$\Delta h^2 = \frac{2S(\omega_{\mathrm{g}})}{\tau V_{I-}(\omega_{\mathrm{g}})}\,. \tag{8.113}$$

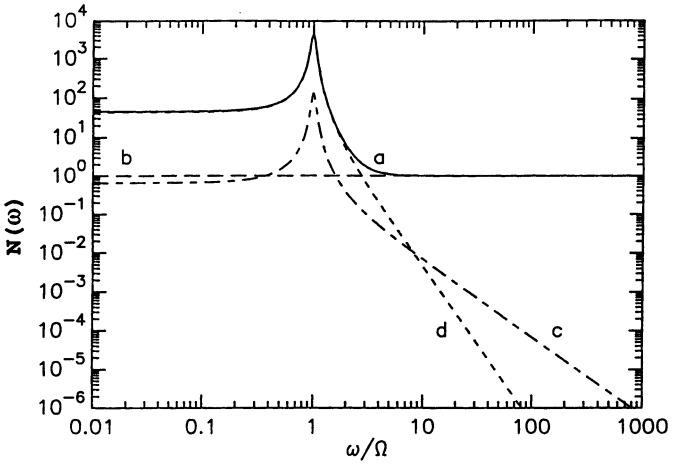

Fig. 8.13 The normalized variance for the fluctuations in the intensity difference versus frequency. The solid line (a) represents the total noise, (b) represents the photon counting noise, (c) represents the mirror noise and (d) represents the radiation pressure noise. The interferometer parameters used are given in Table 8.1

Table 8.1 The values of the experimental parameters used in the graphs

Quantity	Symbol	Value
Mass of mirror	M	10 kg
Mirror characteristic angular frequency	Ω	20πrad s^{-1}
Mirror damping	γ_b	2πrad s^{-1}
Length of cavity	L	4 m
Reflectivity	R	0.98
Laser power	P	10 W
Laser angular frequency	ω_0	3.66×10^5 rad s^{-1}
Gravity-wave-angular frequency	ω_g	2000π rad s^{-1}

We may now substitute the expressions for the signal frequency components $S(\omega_g)$ and the noise at this frequency to obtain an error which depends on the input intensity I (or equivalently the input power $P = 2\hbar\omega_0 I$). The error may then be minimised with respect to I to give minimum detectable displacement $h_{\min}$. In the limit $\omega_g^2 \gg \Gamma^2 + \Omega^2$, the appropriate limit for practical interferometers we find

$$h_{\min}^2 = \frac{\hbar}{32M\omega_g^2 L^2 \tau\Omega}(2\Omega + \Gamma)\,. \tag{8.114}$$

The first term in this expression is due to the light fluctuations whereas the second term is due to the intrinsic quantum noise in the end mirrors. If we neglect the mirror-noise contribution we find the 'standard quantum limit'

$$h_{\mathrm{SQL}} = \frac{1}{L}\left(\frac{\hbar}{16M\omega_g^2\tau}\right)^{1/2}\,. \tag{8.115}$$

In Fig. 8.14 we plot the Δh as a function of input power (8.113), for a measurement time of 1 s, and typical values for the other parameters. Clearly the optimum sensitivity is achieved at rather high input powers.

Can one do better than this, either in achieving the standard quantum limit at lower powers or perhaps even beating the standard quantum limit? As we now show both these results can be achieved by a careful use of squeezed states.

To see now how this might work return to (8.110) and the physical interpretation of each term. Firstly, we note that one might reduce radiation pressure fluctuations (the first term) by using input squeezed light with reduced amplitude fluctuations. Unfortunately, this would increase the overall intensity fluctuations at the detector, i.e. it would increase the photon counting noise. However, as these two terms scale differently with intensity it is possible to apply such a scheme to enable the standard quantum limit to be achieved at lower input power. This is indeed the conclusion of *Caves* [16] in a calculation which focussed entirely on these terms. However, one can actually do better by using squeezed states to induce correlations between the

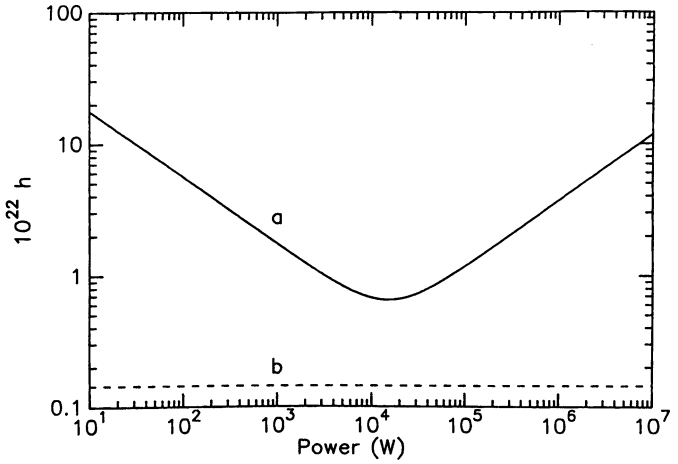

Fig. 8.14 The error in the fractional length change versus input power for a measurement time of one second. Parameters are as in Table 8.1

in-phase and out-of-phase quadratures of the field. In fact, if one chooses the phase of the squeezing (with respect to the input laser) carefully the fifth term in (8.110) can be made negative with a consequent improvement in the overall sensitivity of the device.

We will not present the details of this calculation [20], but summarise the results with reference to Fig. 8.15. Firstly, if we simply squeeze the fluctuations in $\hat{x}^{\text{in}}$ without changing the vacuum correlations between $\hat{x}^{\text{in}}$ and $\hat{y}^{\text{in}}$, the standard quantum

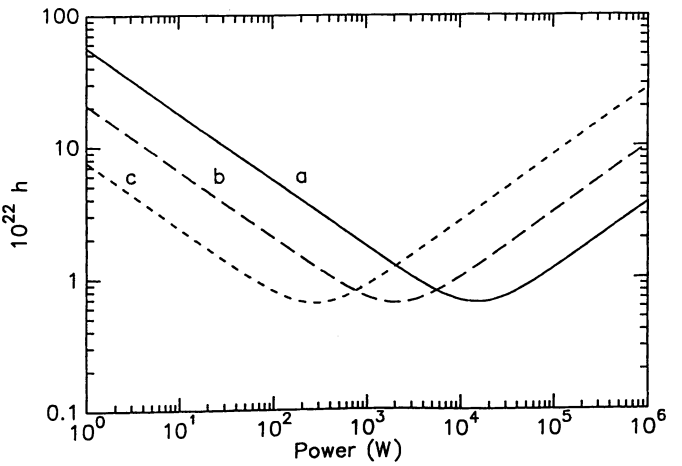

Fig. 8.15 The minimum possible detectable gravitational wave amplitude h as a function of power using amplitude squeezed light at the input and for three different squeeze parameters; (**a**) $r = 0$; (**b**) $r = 1$; (**c**) $r = 2$

limit (8.115) is the optimum sensitivity regardless of the degree of squeezing and it is achieved for the input power

$$P_{\rm ss} = {\rm e}^{-2r} P_{\rm o} \,, \tag{8.116}$$

where r is the squeeze parameter, and $P_{\rm o}$ is the optimum laser power for the system with no squeezing.

However, if one now optimises the phase of the squeezing thereby introducing correlations between $\delta\hat{x}^{\rm in}$ and $\delta\hat{y}^{\rm in}$ we find the optimum sensitivity is achieved with the *same* input power $P_{\rm o}$ as the unsqueezed state, but the optimum sensitivity in the appropriate limit is

$$h^2_{\rm min} \approx \frac{\hbar}{32 M \omega_{\rm g}^2 L^2 \tau \Omega} (2{\rm e}^{-2|r|}\Omega + \Gamma) \,. \tag{8.117}$$

clearly this may be made much smaller than the standard quantum limit. For Lightly squeezed input light the sensitivity is ultimately limited by the intrinsic quantum fluctuations in the positions of the end mirrors. The optimum phase of squeezing is $\pi/4$ which is the angle at which maximum correlation between $\hat{x}^{\rm in}$ and $\hat{y}^{\rm in}$ occurs, i.e., the error ellipse has the same projection onto the in-phase and out-of-phase directions. The exact results are shown in Fig. 8.15 for the same parameters, as employed in Fig. 8.15. Shown is the minimum-possible value of h detectable as a function of power at the optimum phase of squeezing, for three different values of the squeeze parameter. Also exhibited is the noise floor due to the intrinsic quantum fluctuations of the mirror positions.

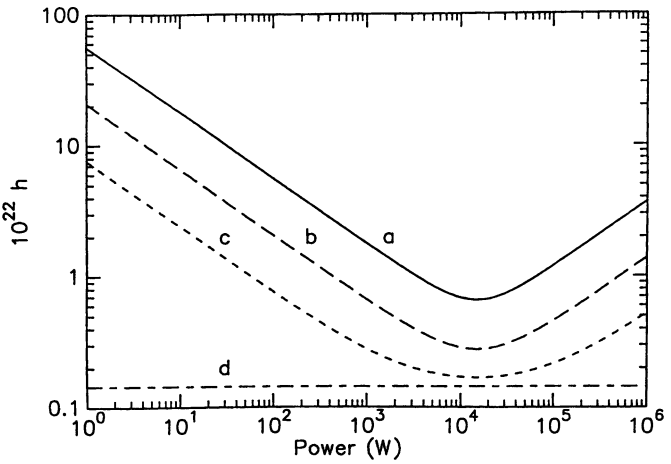

Fig. 8.16 The minimum possible detectable amplitude h as a function of input power when the phase of the input squeezed light is optimized, for three different values of the squeeze parameter (**a**) $r = 0$; (**b**) $r = 1$; (**c**) $r = 2$. Also shown is the mirror noise contribution (**d**)

In summary, the experimentalist can apply a squeezed input to a gravitational wave interferometer in two ways. Either the maximum sensitivity of the device can be greatly increased but achieved at a rather high input power, or the standard quantum limit can be achieved at input powers less threatening to the life of the optical components of the interferometer.

8.3.2 Sub-Shot-Noise Phase Measurements

The second major application of squeezed light is to the detection of very small phase shifts. A Mach–Zehnder interferometer (Fig. 8.17) can be used to determine a phase shift introduced in one arm.

Assuming 50:50 beam splitters the relationship between the input and output field operators is

$$a_{\mathrm{o}} = \mathrm{e}^{\mathrm{i}\theta/2}\left(\cos\frac{\theta}{2}a_i + \sin\frac{\theta}{2}b_i\right) , \tag{8.118}$$

$$b_{\mathrm{o}} = \mathrm{e}^{\mathrm{i}\theta/2}\left(\cos\frac{\theta}{2}b_i + \sin\frac{\theta}{2}a_i\right) , \tag{8.119}$$

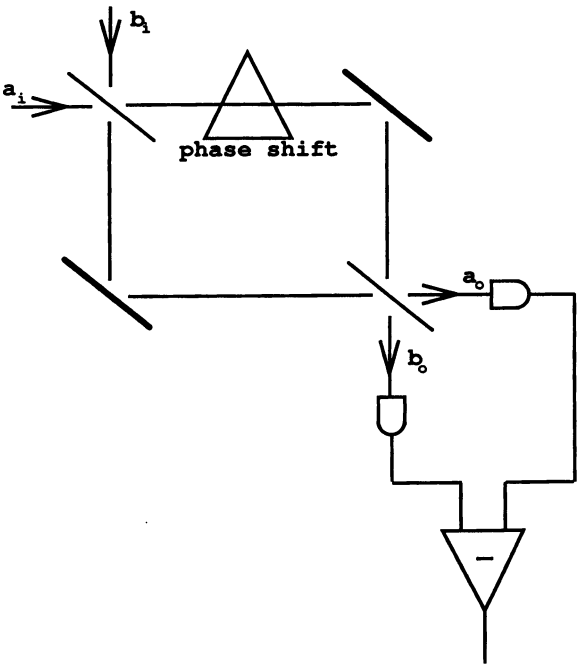

Fig. 8.17 Schematic representation of an experiment designed to measure a phase shift below the shot-noise limit

where θ is the phase difference between the two arms. The two output fields are directed onto two photo-detectors and the resulting currents combined with a 180° power combiner. This realises a measurement of the photon number difference

$$\begin{aligned} c_{\rm o}^{\dagger}c_{\rm o} &= a_{\rm o}^{\dagger}a_{\rm o} - b_{\rm o}^{\dagger}b_{\rm o} \\ &= \cos\theta(a_i^{\dagger}a_i - b_i^{\dagger}b_i) - {\rm i}\sin\theta(a_i b_i^{\dagger} - a_i^{\dagger}b_i)\,. \end{aligned} \tag{8.120}$$

In standard interferometry the input a_i is a stabilised cw laser while b_i is the vacuum state. However, as we shall show, smaller phase changes may be detected if b_i is prepared in a squeezed vacuum state.

Assuming a_i is in the coherent state $|\alpha\rangle$ while b_i is in the squeezed state $|0,\ r\rangle$, the mean and variance of the photon number difference at the output is

$$\langle c_-^{\dagger}c_-\rangle = \cos\theta(|\alpha|^2 - \sinh^2 r) \tag{8.121}$$

$$\begin{aligned} V(c_-^{\dagger}c_-) = {}& \cos^2\theta(|\alpha|^2 + \sinh^2 r\cosh 2r) + \sin^2\theta[|\alpha|^2(1-2\sinh^2 r)] \\ & - \frac{1}{2}(\alpha^2 + \alpha^{*2})\sinh 2r + \sinh^2 r]\,. \end{aligned} \tag{8.122}$$

If we now set $\theta = \pi/2 + \delta\theta$, then when phase shift $\delta\theta$ is zero, the mean signal is zero. That is we operate on a null fringe. The Signal-to-Noise Ratio (SNR) is defined by

$${\rm SNR} = \frac{\langle c_-^{\dagger}c_-\rangle}{\sqrt{V(c_-^{\dagger}c_-)}}\,. \tag{8.123}$$

In the standard scheme $r = 0$ and

$${\rm SNR} = \bar{n}^{1/2}\sin\delta\theta \tag{8.124}$$

where $\bar{n} = |\alpha|^2$. The smallest detectable phase shift is defined to be that phase for which SNR = 1. Thus the minimum detectable phase shift for coherent state interferometry is

$$\delta\theta_{\rm min} = \bar{n}^{-1/2}\,. \tag{8.125}$$

However, if b_i is prepared in a squeezed vacuum state with squeezing in phase with the amplitude α we find for moderate squeezing ($|\alpha|^2 \gg \sinh^2 r$)

$${\rm SNR}_{\rm ss} = \bar{n}^{1/2}{\rm e}^{r}\sin\delta\theta \tag{8.126}$$

and thus the minimum detectable phase change is

$$\delta\theta_{\rm min} = \bar{n}^{1/2}{\rm e}^{r}\,. \tag{8.127}$$

The minimum detectable phase change may thus be much smaller than for coherent state interferometry, provided we choose $r < 0$ i.e. *phase squeezing*.

Such an enhancement has been reported by *Xiao* et al. [22] in an experiment on the measurement of phase modulation in a Mach Zehnder interferometer. They reported on an increase in the signal-to-noise ratio of 3 dB relative to the shot-noise limit when squeezed light from an optical parametric oscillator is injected into a port of the interferometer. A comparison of the fluctuations in the difference current for the cases of squeezed and a vacuum input is shown in Fig. 8.18. A similar experiment was performed by *Grangier* et al. [23] employing a polarization interferometer which is equivalent to a Mach–Zehnder scheme. In their experiment an enhancement factor of 2 dB was achieved.

8.3.3 Quantum Information

Squeezed states are being applied to new protocols in quantum information which we discuss in. In Chap. 16. Quantum information is concerned with communication and computational tasks enabled by quantum states of light, including squeezed states. One such application is quantum teleportation in which an unknown quantum state is transferred from one subsystem to another using the correlations inherent in a two mode squeezed state.

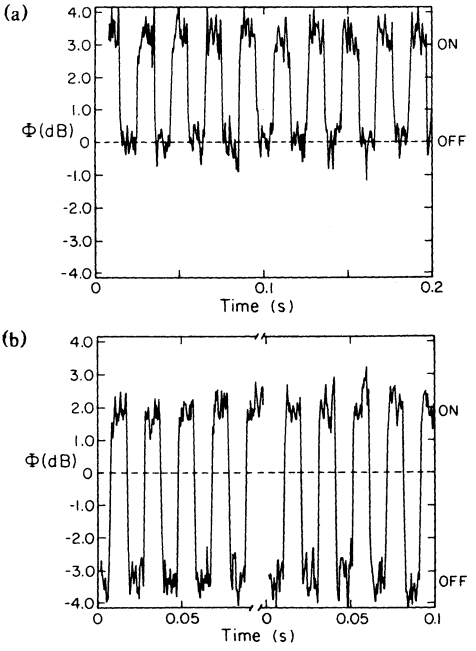

Fig. 8.18 A comparison of the level of fluctuations in the differenced-photocurrent for a Mach–Zehnder interferometer versus time as the phase difference is varied at a frequency of 1.6 MHz. Curve in (a) is for the case of vacuum state input, curve (b) uses squeezed state input. The dashed line gives the vacuum level with no phase modulation [21]

Exercises

8.1 One of the input modes of a beam splitter, with transmitivity T, is prepared in a coherent state, $|\alpha\rangle$ and the other in a squeezed vacuum state $|0, r\rangle$. Show that in the limit $T \to 1,\ |\alpha| \to \infty$ with $\sqrt{(1-T)}|\alpha| = \beta$ fixed, one of the output states is a squeezed state with a coherent amplitude β.

8.2 Calculate the squeezing spectrum for parametric oscillation in a cavity that has different losses at each mirror for the fundamental frequency, ω_1.

8.3 Calculate the spectrum of fluctuations in the difference intensity, $I_1 - I_2$, if an intracavity loss is present at the idler frequency.

8.4 Two photon absorption inside a cavity can be modeled by coupling the cavity mode to a bath via the interaction Hamiltonian

$$\mathscr{H} = a^2\Gamma^\dagger + (a^\dagger)^2\Gamma$$

where Γ is a reservoir operator and the reservoir is at zero temperature. Determine the squeezing spectrum.

References

1. P.D. Drummond, K.J. McNeil, D.F. Walls: Optica Acta **28**, 211 (1981)
2. M.J. Collett, C.W. Gardiner: Phys. Rev. **30**, 1386 (1984)
3. M.J. Collett, D.F. Walls: Phys. Rev. A **32**. 2887 (1985)
4. L.A. Wu, M. Xiao, H.J. Kimble: J. Opt. Soc. Am. B **4**, 1465 (1987)
5. P.K. Lam, T.C. Ralph, B.C. Buchler, D. E. McClelland, H.-A. Bachor, J. Gao: J. Opt. B: Quantum Semi-class. Opt. **1**, 469 (1999)
6. A.S. Lane, M.D. Reid, D.F. Walls: Phys. Rev. A **38**, 788 (1988)
7. S. Reynaud, C. Fabre, E. Giacobino: J. OPt. Soc Am. B **4**, 1520 (1987)
8. A.S. Lane, M.D. Reid, D.F. Walls: Phys. Rev. Lett. **60**, 1940 (1988)
9. A. Heidmann, R.J. Horowicz, S. Reynaud, E. Giacobino, C. Fabre: Phys. Rev. Lett. **59**, 2555 (1987)
10. Jiangrui Gao, Fuyun Cui, Chenyang Xue, Changde Xie, Peng Kunchi: Opts. Letts. **23**, 870 (1998)
11. O. Aytür, P. Kumar: Phys. Rev. Lett. **65**, 1551 (1990)
12. S.F. Pereira, M. Xiao, H.J. Kimble, J.L. Hall: Phys. Rev. A, **38**, 4931 (1989)
13. A. Sizman, R.J. Horowicz, G. wagner, G. Leuchs: Opt. Comms. **80**, 138 (1990)
14. R. Paschotta, M. Collett, P. Kurz, K. Fiedler, H.A. Bachor, J. Mlynek: Phys. Rev. Lett. **72**, 3807 (1994)
15. D.K. Serkland, P. Kumar, M.A. Arbore, M.M. Fejer: Opts. Letts., **22**, 1497 (1997)
16. C.M. Caves: Phys. Rev. Lett. **45**, 75 (1980)
17. W.G. Unruh: *In Quantum Optics, Experimental Gravitation and Measurement Thery*, ed. by P. Meystre, M.O. Scully (Plenum, New York 1983) p.647
18. R.S. Bondurant, J.H. Shapiro: Phys. Rev. D **30**, 2548 (1984)
19. M.T. Jaekel, S. Reynaud: Europhys. Lett. **13**, 301 (1990)
20. A.F. Pace, M.J. Collett, D.F. Walls: Phys. Rev. A **47**, 3173 (1993)
21. C.W. Misner, A.S. Thorne, J.A. Wheller: *Gravitation* (Freeman, San Francisco 1973)
22. M. Xiao, L.A. Wu, H.J. Kimble: Phys. Rev. Lett. **59**, 278 (1987)
23. P. Grangier, R.E. Slusher, B. Yurke, A. La Porta: Phys. Rev. Lett. **59**, 2153 (1987)

Further Reading

Bachor, H.A., J.C. Ralph: *A Guide to Experiments in Quantum Optics* (Wiley-VCH, 2004)
Giacobino, E., C. Fabre (guest eds.): *Quantum noise reduction in optical systems-experiments*, Appl. Phys. B **55**(3) (1992)
Kimble, H.J., D.F. Walls (guest eds.): *Special Issue on Squeeze States of the Electromagnetic Field*, J. Opt. Soc. Am. B **4**(10) (1987)